J. Phys.: Condens. Matter **25** (2013) 416008 (11pp) doi:10.1088/0953-8984/25/41/416008

A Mössbauer effect study of single crystals of the non-superconducting parent compound $Fe_{1.09}Te$ and the superconductor $FeSe_{0.4}Te_{0.6}$

Zbigniew M Stadnik[1], Pu Wang[2], Jan Żukrowski[3], Takashi Noji[4] and Yoji Koike[4]

[1] Department of Physics, University of Ottawa, Ottawa, Ontario, K1N 6N5, Canada
[2] Key Laboratory of Extreme Conditions Physics, The Institute of Physics, Chinese Academy of Sciences, Beijing 100190, People's Republic of China
[3] Solid State Physics Department, Faculty of Physics and Applied Computer Science, AGH University of Science and Technology, 30-059 Kraków, Poland
[4] Department of Applied Physics, Tohoku University, Sendai 980-8579, Japan

E-mail: stadnik@uottawa.ca

Received 5 June 2013, in final form 8 August 2013
Published 24 September 2013
Online at stacks.iop.org/JPhysCM/25/416008

Abstract
The results of a ^{57}Fe Mössbauer spectroscopy study between 2.0 and 297 K of the parent compound $Fe_{1.09}Te$ and the superconductor $FeSe_{0.4}Te_{0.6}$ are reported. It is shown that in both compounds the magnitude of the quadrupole splitting increases with decreasing temperature and is well described by a $T^{3/2}$ power-law relation. The presence of incommensurate spin-density-wave antiferromagnetism in $Fe_{1.09}Te$ is demonstrated, with the Néel temperature $T_N = 71.1(6)$ K. A theoretical prediction (Zhang *et al* 2009 *Phys. Rev.* B **79** 012506) of the Fe magnetic moment at the 2*c* sites being significantly larger than that at the 2*a* sites in the parent compound is confirmed experimentally by showing that these moments at 4.4 K are, respectively, 3.20(4) and 1.78(3) μ_B. The absence of magnetic order in $FeSe_{0.4}Te_{0.6}$ down to 2.0 K is confirmed. The Debye temperatures of $Fe_{1.09}Te$ and $FeSe_{0.4}Te_{0.6}$ are found to be 290(1) and 233(1) K, respectively.

(Some figures may appear in colour only in the online journal)

1. Introduction

There are two recently discovered Fe-chalcogenide superconductor series, $Fe_{1+x}Te_{1-y}Se_y$ and $Fe_{1+x}Te_{1-y}S_y$ [1–5]. The parent compound for these two series, $Fe_{1+x}Te$, is non-superconducting. It was realized a long time ago [6, 7] that iron monotelluride cannot be synthesized in the simple stoichiometry FeTe but that it can exist over a small range of Fe-excess non-stoichiometry as $Fe_{1+x}Te$. The presence of a well-defined maximum at 63 K in the magnetic susceptibility of $Fe_{1.05}Te$ [8], and a lambda-shaped discontinuity at the same temperature in the specific heat of $Fe_{1.11}Te$ [9], clearly established the antiferromagnetic ordering of Fe magnetic moments in the $Fe_{1+x}Te$ system. This antiferromagnetic nature of the ordering of the Fe magnetic moments of magnitude 2.07(7) μ_B was confirmed by the first neutron diffraction study on $Fe_{1.125}Te$ [10]. A partial substitution of Te in the parent compound $Fe_{1+x}Te$ by Se or S induces superconductivity while suppressing antiferromagnetic order [1–5].

Following the discovery of superconductivity in the $Fe_{1+x}Te_{1-y}Se_y$ and $Fe_{1+x}Te_{1-y}S_y$ series, the magnetic properties of the parent compound $Fe_{1+x}Te$ have been re-investigated in detail. On the theoretical side, density

functional studies within the context of the itinerant model indicate that in the model compound $Fe_{1.125}Te$ the interstitial excess Fe atoms located at the 2*c* sites should carry a significant magnetic moment (2.4–2.5 μ_B) that is much larger than the magnetic moment (1.6–1.8 μ_B) of Fe atoms located at the 2*a* sites [11]. Recent neutron diffraction studies [12–17] of the parent compound $Fe_{1+x}Te$ show that the antiferromagnetic order can be commensurate bi-collinear or incommensurate depending upon *x*—the amount of excess Fe. The Fe magnetic moment was shown to be pointing mostly along the *b*-axis (in the commensurate bi-collinear structure) and its value (assumed to be the same at the 2*a* and the interstitial 2*c* sites) was found to lie in a rather wide range from 1.4 to 2.54 μ_B [12–17].

In this paper we perform a detailed ^{57}Fe Mössbauer spectroscopy study of single crystals of the parent compound $Fe_{1.09}Te$ and the superconductor $FeSe_{0.4}Te_{0.6}$ with the critical temperature $T_c = 14.2$ K [18, 19]. Part of the motivation for this study is to test the theoretical prediction [11] of Fe magnetic moments at the 2*c* sites being significantly larger than those at the 2*a* sites in the parent compound $Fe_{1+x}Te$ and to determine the nature of antiferromagnetic ordering (commensurate versus incommensurate) in this compound. Previous ^{57}Fe Mössbauer spectroscopy studies [20–24] of $Fe_{1+x}Te$ were all done on polycrystalline specimens and mainly at room temperature. As discussed below, the analyses of Mössbauer spectra in some of these studies are questionable. We are not aware of any ^{57}Fe Mössbauer spectroscopy study of the $FeSe_{0.4}Te_{0.6}$ superconductor.

2. Experimental methods

The single crystals of $Fe_{1.09}Te$ and $FeSe_{0.4}Te_{0.6}$ used in this study were grown by the Bridgman method [19]. They were annealed at 673 K for 100 h in vacuum ($\sim 10^{-4}$ Pa) using an oil-diffusion pump. Annealing of the as-grown single crystals of the Fe–Te–Se system is very important, as it leads to significant enhancement of superconductivity via a more homogeneous distribution of Se and Te, the relaxation of lattice distortion and the elimination of excess Fe [25–28]. The chemical composition of the crystals was determined by inductively coupled plasma atomic emission spectroscopy [19].

X-ray diffraction measurements on ground single crystals were performed at 298 K in the Bragg–Brentano geometry on a PANanalytical X'Pert scanning diffractometer using Cu Kα radiation in the 2θ range 10°–100° in steps of 0.02°. The $K\beta$ line was eliminated by using a Kevex PSi2 Peltier-cooled solid-state Si detector.

The ^{57}Fe Mössbauer measurements were conducted using a standard Mössbauer spectrometer operating in the sine mode and a ^{57}Co(Rh) source at room temperature. The spectrometer was calibrated with a 6.35-μm-thick α-Fe foil [29] and the spectra were folded. The single crystals of $Fe_{1.09}Te$ and $FeSe_{0.4}Te_{0.6}$ are in the form of *ab*-plane plates with the tetragonal *c*-axis perpendicular to the plate. They could easily be cleaved, using a razor blade, into many flat plates of $\sim$100 μm thickness. The Mössbauer absorber was made from several such plates by attaching them with Apiezon N grease to a high-purity, 8 μm-thick Al disk container to ensure a uniform temperature over the whole absorber. The plates slightly overlapped in order to avoid gaps between them. The direction of the γ-rays was perpendicular to the surface of the plates, i.e., parallel to the *c*-axis. The Mössbauer absorber thickness of 100 μm corresponds to an effective thickness parameter [30] $T = 13 f_a$, where f_a is the Debye–Waller factor of the absorber. Since $T > 1$, the resonance line shape of the Mössbauer spectrum was described using a transmission integral formula [31]. The source linewidth $\Gamma_s = 0.12$ mm s^{-1} and the background-corrected Debye–Waller factor of the source $f_s^* = 0.40$ were used in the fits of the Mössbauer spectra [31]. As the electric quadrupole interaction is significantly smaller than the magnetic dipole interaction in the parent compound, the ^{57}Fe Zeeman spectra at temperatures below T_N were analyzed using a first-order perturbation treatment [30].

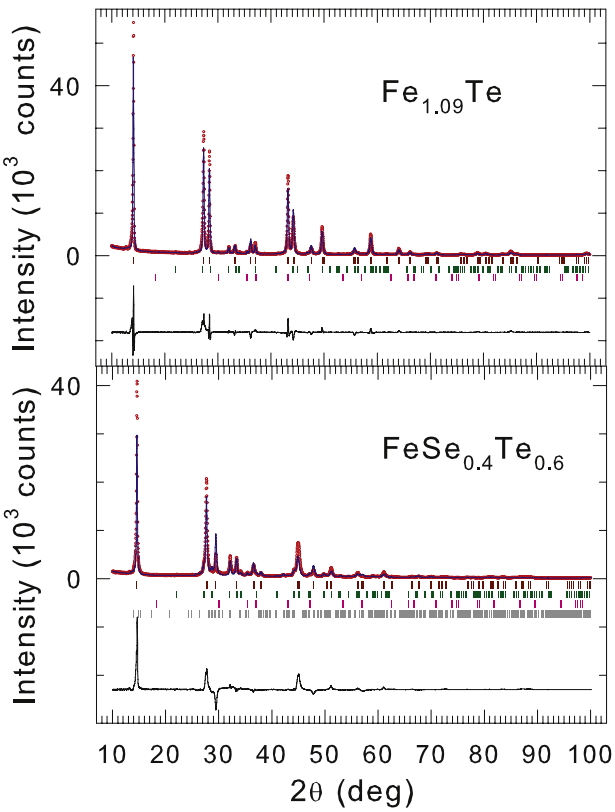

Figure 1. Powder x-ray diffraction patterns of $Fe_{1.09}Te$ and $FeSe_{0.4}Te_{0.6}$ at 298 K. The experimental data are denoted by open circles (red), while the lines (blue) through the circles represent the result of the Rietveld refinement. The rows of tick marks show the Bragg peak positions for the main phase (dark red), and the impurity phases of Fe_2Te (dark green), Fe_3O_4 (pink), and Fe_7Se_8 (dark gray). The lower solid lines represent the difference curves between experimental and calculated patterns.

3. Experimental results and discussion

The room-temperature powder x-ray diffraction patterns of $Fe_{1.09}Te$ and $FeSe_{0.4}Te_{0.6}$ are shown in figure 1. At high

Table 1. Refined structural parameters of $Fe_{1.09}Te$ and $FeSe_{0.4}Te_{0.6}$ with the space group $P4/nmm$ (No. 129) at 298 K.

Atom	Site	Point symmetry	Occupancy	x	y	z
Fe	$2a$	$\bar{4}m2$	1.0	$\frac{3}{4}$	$\frac{1}{4}$	0
Fe	$2c$	$4mm$	0.09(1)	$\frac{1}{4}$	$\frac{1}{4}$	0.679(22)
Te	$2c$	$4mm$	1.0	$\frac{1}{4}$	$\frac{1}{4}$	0.280(19)
$Fe_{1.09}Te$, $a = 3.8218(1)$ Å, $c = 6.2844(1)$ Å						
Fe	$2a$	$\bar{4}m2$	1.0	$\frac{3}{4}$	$\frac{1}{4}$	0
Te	$2c$	$4mm$	0.6(1)	$\frac{1}{4}$	$\frac{1}{4}$	0.279(21)
Se	$2c$	$4mm$	0.4(1)	$\frac{1}{4}$	$\frac{1}{4}$	0.279(21)
$FeSe_{0.4}Te_{0.6}$, $a = 3.8020(2)$ Å, $c = 6.0620(3)$ Å						

temperatures, the studied compounds have a tetragonal crystal structure with the space group $P4/nmm$ (No. 129) [14]. The structural parameters of $Fe_{1.09}Te$ and $FeSe_{0.4}Te_{0.6}$ obtained from the Rietveld refinement (figure 1) in this space group are listed in table 1. The values of these parameters compare well with the corresponding values reported earlier [13–16, 32]. As determined from the Rietveld refinement (figure 1), the $Fe_{1.09}Te$ specimen contains second phases of $FeTe_2$ (space group $Pnmm$) in the amount of 2.5(4) wt% and Fe_3O_4 (space group $Fd\bar{3}m$) in the amount of 1.2(2) wt%, whereas the $FeSe_{0.4}Te_{0.6}$ specimen contains second phases of $FeTe_2$ in the amount of 3.1(6) wt%, Fe_3O_4 in the amount of 1.4(3) wt%, and Fe_7Se_8 (space group $P3_121$) in the amount of 1.3(3) wt%. The studied parent compound is expected to experience a structural phase transition at ∼67 K [14], changing the symmetry from tetragonal $P4/nmm$ to orthorhombic $P2_1/m$.

The room-temperature ^{57}Fe Mössbauer spectrum of $Fe_{1.09}Te$ measured in a large velocity range (figure 2(a)) confirms the presence of a small amount of magnetite [33]. The presence of $FeTe_2$ could not be confirmed, as its quadrupole-doublet spectrum [34] overlaps with the dominant three-quadrupole-doublet spectrum (discussed below) of $Fe_{1.09}Te$. The room-temperature ^{57}Fe Mössbauer spectrum of $Fe_{1.09}Te$ measured in a small velocity range (figure 2(b)) is in the form of an asymmetric, broadened quadrupole doublet. At first sight it would appear that this spectrum should be fitted with two elemental quadrupole doublets corresponding to Fe atoms at the $2a$ and $2c$ sites (table 1). A careful analysis of this spectrum shows that no satisfactory fit can be obtained with either one quadrupole doublet or two elemental quadrupole doublets. A perfect fit of this spectrum (figure 2(b)) requires three elemental quadrupole doublets (in this fit the low-intensity inner lines of six-line Zeeman patterns from magnetite are included). This observation of the necessity of three doublets to account for the shape of the room-temperature Mössbauer spectrum of $Fe_{1+x}Te$ was made a long time ago [21]. The fit of this spectrum with three quadrupole doublets yields the following parameters: the absorber linewidth Γ_a, the center shift δ (relative to α-Fe at 298 K), the quadrupole splitting $\Delta = \frac{1}{2}eQV_{zz}$ (where e is the proton charge, Q is the electric quadrupole moment of the ^{57}Fe nucleus [35], and V_{zz} is the principal component of

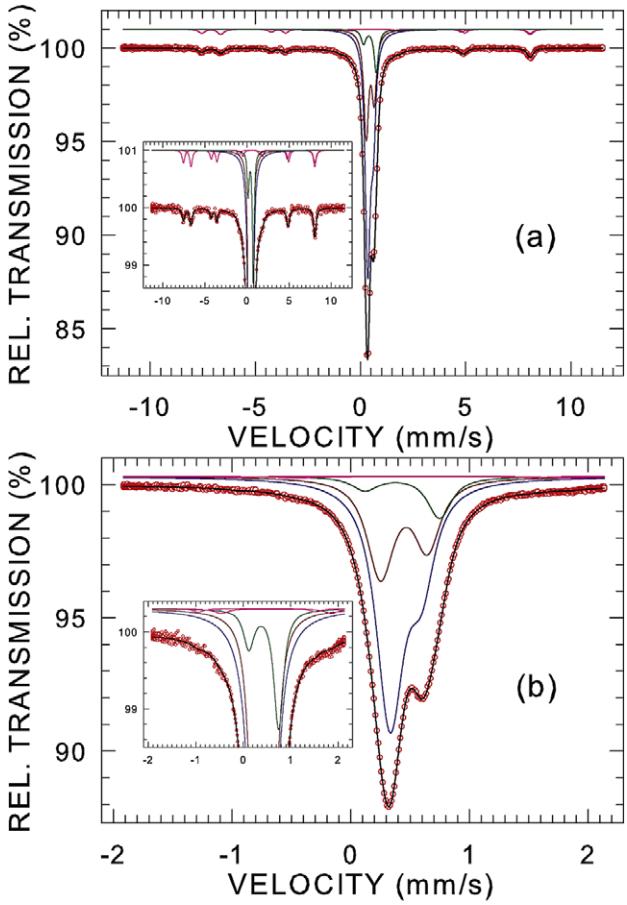

Figure 2. ^{57}Fe Mössbauer spectra of $Fe_{1.09}Te$ at 297.3 K, measured in a large (a) and small (b) velocity range, fitted (black solid lines) with three asymmetric quadrupole doublets (blue, dark red, and dark green solid lines) and Zeeman patterns (pink solid lines) originating from Fe_3O_4, as described in the text. The insets show the spectra with an enlarged vertical scale. The zero-velocity origin is relative to α-Fe at room temperature.

the electric field gradient tensor), the angle θ between V_{zz} and the γ-ray propagation direction, and the spectral area A [30]. The values of these parameters corresponding to these three quadrupole doublets are listed in table 2. What is the origin of these three, rather than the two expected quadrupole doublets? As was shown elegantly by Ward and McCann [21], the first

Table 2. Parameters obtained from the fits of the room-temperature Mössbauer spectra of $Fe_{1.09}Te$ (figure 2(b)) and $FeSe_{0.4}Te_{0.6}$ (figure 9(b)).

Doublet	Γ_a (mm s^{-1})	δ (mm s^{-1})	Δ (mm s^{-1})	θ (deg)	A (%)
Doublet 1	0.098(3)	0.463(2)	−0.264(4)	0(1)	64.1(9)
Doublet 2	0.099(4)	0.448(1)	0.395(7)	73(1)	27.7(8)
Doublet 3	0.075(6)	0.434(3)	0.628(8)	0(1)	8.2(5)
$Fe_{1.09}Te$, $T = 297.3$ K					
Doublet	0.115(2)	0.459(1)	−0.303(1)	18.3(3)	100
$FeSe_{0.4}Te_{0.6}$, $T = 297.1$ K					

doublet is due to Fe atoms at 2*a* sites with no Fe nearest neighbors at 2*c* sites, the second doublet originates from Fe atoms at 2*a* sites with 1, 2, 3, or 4 Fe nearest neighbors at 2*c* sites, and the third doublet is due to Fe atoms at 2*c* sites. The probabilities of these three configurations of Fe atoms in a compound $Fe_{1+x}Te$ are $(1-x)^4/(1+x)$, $[1-(1-x)^4]/(1+x)$, and $x/(1+x)$, respectively. For the compound studied here ($x = 0.09$), these probabilities are 0.629, 0.288, and 0.083. The fitted spectral areas A_1, A_2, and A_3 (table 2) are in an excellent agreement with these probabilities, thus confirming the correctness of the three-quadrupole-doublet model. It should be emphasized here that the above analysis of the Mössbauer spectrum of a single-crystal $Fe_{1.09}Te$ absorber allows us to determine unequivocally the signs of Δ_i. The values of θ_1 and θ_3 derived from the fit confirm that, as expected from the point symmetries of the 2*a* and 2*c* sites (table 1), the principal axis of the electric field gradient tensor at these sites is along the crystallographic *c*-axis.

We note here that the analysis of room-temperature Mössbauer spectra of polycrystalline $Fe_{1+x}Te$ in recent reports [23, 24] is problematic. The observed Mössbauer spectra are in the form of a pair of broadened lines, with the higher-velocity line having a slightly lower intensity than the lower-velocity line [23, 24]. The asymmetry of the observed spectrum was accounted for in [23] by fitting it with a symmetric quadrupole-doublet component (corresponding to Fe at the 2*a* sites) and a single-line component (corresponding to Fe at the 2*c* sites) located at the lower-intensity line position of the experimental spectrum. The asymmetry of the observed spectrum is caused by preferred orientation (texture) in the polycrystalline Mössbauer absorber (the tendency of the polycrystalline grains of a layer-structure compound to align themselves predominantly with the *c*-axis perpendicular to the plane of the absorber), and therefore such a fit is unwarranted, i.e., the single-line component is an artifact which has no relation to Fe atoms at the 2*c* sites. Similarly, the room-temperature Mössbauer spectra of polycrystalline $Fe_{1+x}Te$ were fitted in [24] with either two quadrupole doublets and a single-line component, or three-quadrupole-doublet components, with no justification of the origin of these components.

Figure 3 shows the ^{57}Fe Mössbauer spectra of $Fe_{1.09}Te$ measured at temperatures above the Néel temperature T_N. Excellent fits of these spectra are obtained with the three-quadrupole-doublet model discussed above. The values of Δ_i derived from the fits of these spectra and of the spectrum in figure 2(b) are shown in figures 4(a)–(c). A clear increase in the magnitude of Δ_i with decreasing temperature (figures 4(a)–(c)) is found. Such a temperature dependence of Δ has been observed in many non-cubic metallic compounds [36] and is well described by the empirical equation

$$\Delta(T) = \Delta(0)(1 - BT^{3/2}), \tag{1}$$

where $\Delta(0)$ is the value of Δ at 0 K and B is a constant. The fit of the $\Delta_i(T)$ data (figures 4(a)–(c)) to equation (1) gives $\Delta_1(0) = -0.344(3)$ mm s^{-1}, $B_1 = 4.71(24) \times 10^{-5}$ K$^{-3/2}$, $\Delta_2(0) = 0.414(5)$ mm s^{-1}, $B_2 = 1.43(40) \times 10^{-5}$ K$^{-3/2}$, and $\Delta_3(0) = 0.664(4)$ mm s^{-1}, $B_3 = 0.902(169) \times 10^{-5}$ K$^{-3/2}$. The values of B_i are similar to those found for other non-cubic compounds [36].

The absorption spectral area A of a Mössbauer spectrum is proportional to the absorber Debye–Waller factor f_a, which is given in the Debye theory by [30]

$$f_a(T) = \exp\left\{-\frac{3}{4}\frac{E_\gamma^2}{Mc^2 k_B \Theta_D}\left[1 + 4\left(\frac{T}{\Theta_D}\right)^2 \int_0^{\Theta_D/T} \frac{x\,dx}{e^x - 1}\right]\right\}, \tag{2}$$

where M is the mass of the Mössbauer nucleus, c is the speed of light, E_γ is the energy of the Mössbauer transition, and Θ_D is the Debye temperature. Figure 4(d) shows the temperature dependence of the spectral area A derived from the fits of the Mössbauer spectra in figures 2(b) and 3. The fit of the experimental dependence $A(T)$ (figure 4(d)) to equation (2) gives $\Theta_D = 290(1)$ K. The value of Θ_D found here is much larger than the reported Θ_D values of 179 K for $Fe_{1.09}Te$ [26] and 141 K for $Fe_{1.05}Te$ [37] derived from specific-heat measurements.

The ^{57}Fe Mössbauer spectrum of $Fe_{1.09}Te$ at 4.4 K, i.e., much below T_N, is shown in figure 5(a). Its majority central component due to Fe atoms at the 2*a* sites is in the form of a complex Zeeman-like pattern which is completely different from the standard six-line Zeeman pattern expected for an antiferromagnet [30]. This complex pattern must result from the distribution of the hyperfine magnetic fields which arises from the incommensurate modulation of the antiferromagnetic structure, that is, from the incommensurate spin density wave (SDW) [38–40]. For a collinear antiferromagnetic structure

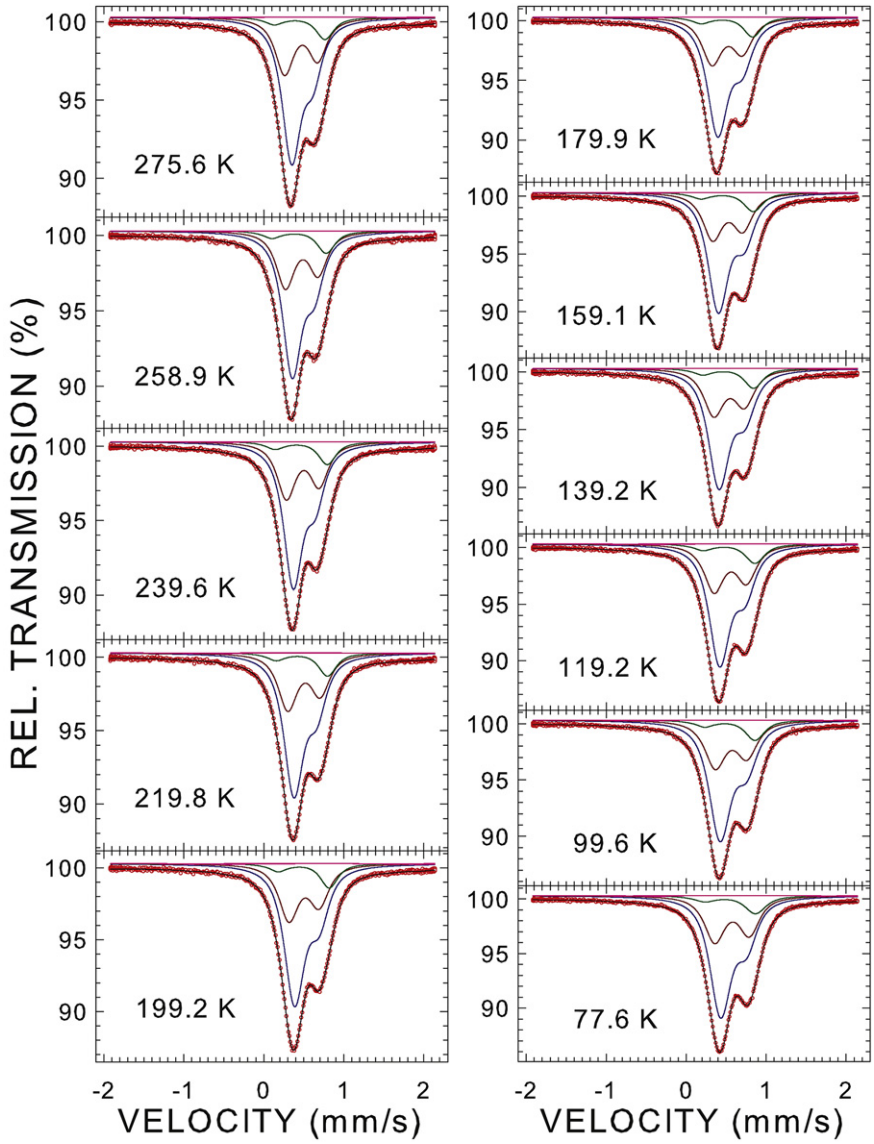

Figure 3. ^{57}Fe Mössbauer spectra of $Fe_{1.09}Te$ at the indicated temperatures fitted (black solid lines) with three asymmetric quadrupole doublets (blue, dark red, and dark green solid lines) and Zeeman patterns (pink solid lines) originating from Fe_3O_4, as described in the text. The zero-velocity origin is relative to α-Fe at room temperature.

(the Fe magnetic moments are aligned antiferromagnetically along the orthorhombic b-axis) and collinearity of the Fe magnetic moment and the hyperfine magnetic field H, one can describe the amplitude of the SDW (the hyperfine magnetic field H) along the x-direction parallel to the wavevector $\mathbf{q}$ as a series of odd harmonics [39, 40],

$$H(qx) = \sum_{i=1}^{n} h_{2i-1} \sin[(2i-1)qx], \qquad (3)$$

where h_{2i-1} is the amplitude of the $(2i-1)$th harmonic, q is the wavenumber of the SDW, x is the relative position of the Fe atom along the direction of SDW propagation, and n denotes the maximum number of harmonics; the periodicity of the SDW demands that $0 \leq qx \leq 2\pi$. A Mössbauer spectrum is then fitted to a set of six-line Zeeman patterns corresponding to H values calculated from equation (3) for discrete qx values from the range $\langle 0, 2\pi \rangle$. We assume the same values of δ and the electric quadrupole shift [30] ε for each elementary Zeeman pattern. The resulting distribution $P(H)$ can then be calculated from the amplitudes h_{2i-1} determined from the fit. The average value of H given by equation (3) is obviously zero, and so the root-mean-square value of H can be obtained from the expression $H_{\mathrm{rms}} = \sqrt{\frac{1}{2}\sum_{i=1}^{n} h_{2i-1}^2}$. The square of H_{rms} is proportional to the intensity of the magnetic Bragg peak in neutron diffraction. Hence, H_{rms} is proportional to the magnetic moment μ_{Fe} of the Fe atoms. The spectrum in figure 5(a) is thus fitted with a SDW pattern due to Fe atoms at $2a$ sites, a six-line Zeeman pattern due to Fe atoms at $2c$ sites, Zeeman patterns originating from the Fe_3O_4 impurity, and an asymmetric quadrupole doublet originating from the $FeTe_2$ impurity. A good fit could be achieved using $n = 6$ harmonics (*vide infra*) with the resulting shape of the SDW shown in figure 5(b) and the corresponding distribution $P(H)$ shown in figure 5(c). The parameters of the SDW component

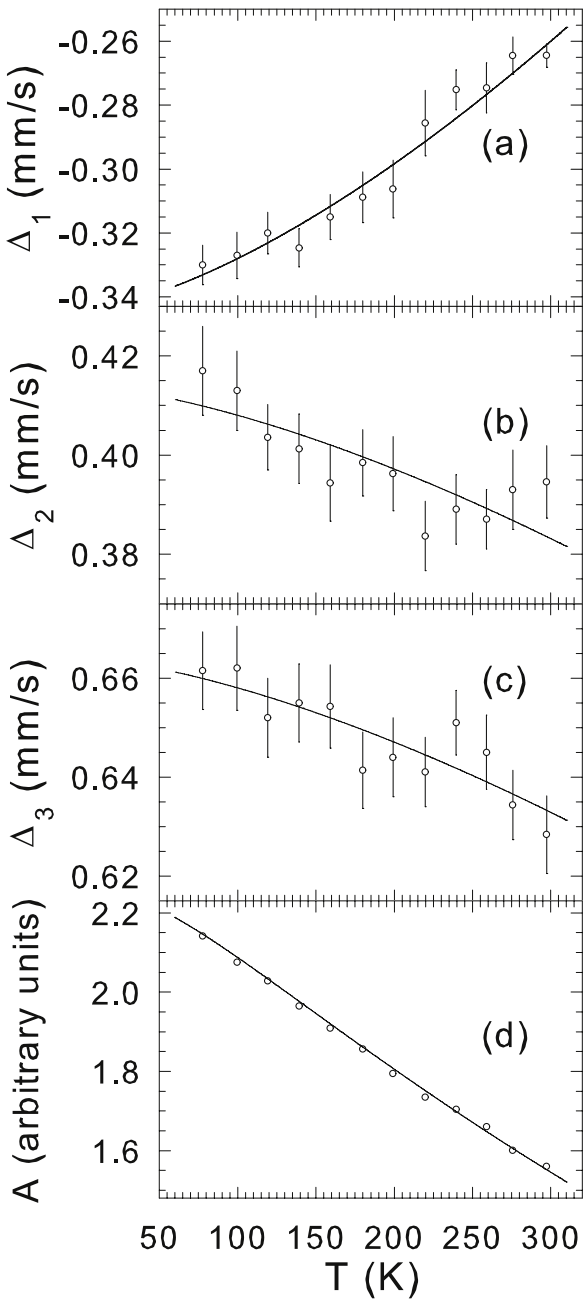

Figure 4. Temperature dependence of (a)–(c) the quadrupole splittings Δ_i ($i = 1, 2, 3$) and (d) the absorption spectral area A of $Fe_{1.09}Te$. The solid lines are the fits to equation (1) in (a)–(c) and to equation (2) in (d), as explained in the text.

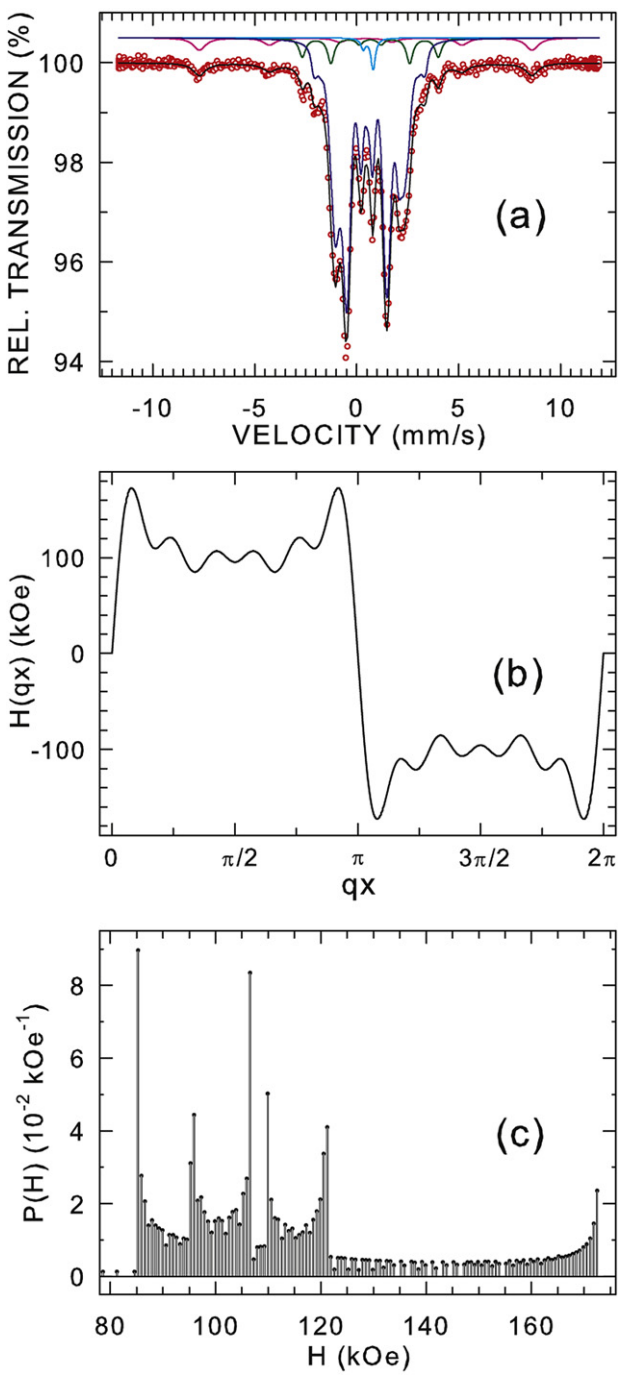

Figure 5. (a) ^{57}Fe Mössbauer spectrum of $Fe_{1.09}Te$ at 4.4 K fitted (black solid line) with a complex Zeeman-like pattern due to Fe atoms at 2*a* sites resulting from incommensurate modulation of the hyperfine magnetic field (blue solid line), a Zeeman pattern due to Fe atoms at 2*c* sites (dark green solid line), Zeeman patterns (pink solid line) originating from the Fe_3O_4 impurity, and an asymmetric quadrupole doublet (cyan solid line) originating from the $FeTe_2$ impurity, as described in the text. (b) The shape of the SDW resulting from incommensurate modulation of the hyperfine magnetic field. (c) The hyperfine magnetic field distribution resulting from incommensurate modulation of the hyperfine magnetic field.

derived from the fit are: $\delta = 0.562(2)$ mm s^{-1}, the maximum value of the hyperfine magnetic field $H_{max} = 172.6(5)$ kOe, the average value of the hyperfine magnetic field derived from the $P(H)$ distribution $\bar{H} = 111.5(4)$ kOe, and $H_{rms} = 115.0(5)$ kOe. The values of δ and H corresponding to the six-line Zeeman component due to Fe atoms at the 2*c* sites are 0.666(22) mm s^{-1} and 206.6(2.9) kOe. This experimental result of H_{rms} being significantly smaller than H supports the theoretical prediction [11] that the magnetic moment of Fe atoms located at 2*a* sites should be much smaller than the magnetic moment of Fe atoms located at 2*c* sites. One can estimate the on-site μ_{Fe} from the measured H since, to a first approximation, H is proportional to μ_{Fe} through the relation $H = a\,\mu_{Fe}$, where the value of the proportionality constant a

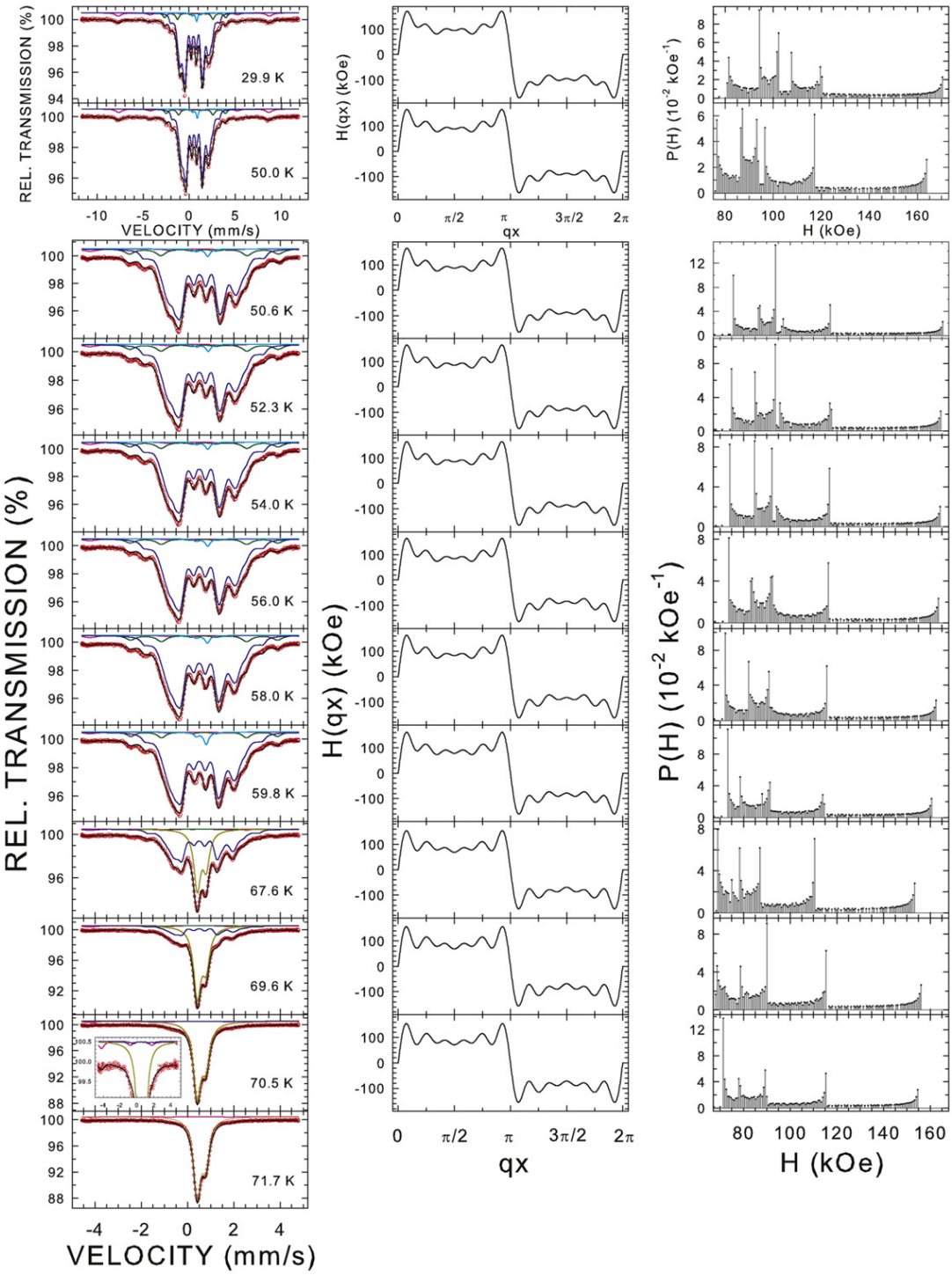

Figure 6. ^{57}Fe Mössbauer spectra of $Fe_{1.09}Te$ at the indicated temperatures fitted (solid black lines) with several component patterns, as described in the text (left panel), the corresponding shapes of the SDW (middle panel), and the resulting hyperfine magnetic field distributions (right panel).

is compound specific [41]. To convert H to μ_{Fe}, a = 64.6 kOe/μ_B was used. This value of a was obtained from H_{rms} = 115.0(5) kOe found here and μ_{Fe}(15 K) = 1.78(3) μ_B determined from a neutron diffraction study of $Fe_{1.05}Te$ [16]. Thus, the values of μ_{Fe} at the 2a and 2c sites are 1.78(3) and 3.20(4) μ_B, respectively.

Figure 6 displays the ^{57}Fe Mössbauer spectra of $Fe_{1.09}Te$ measured at other temperatures below T_N and the Mössbauer spectrum at 71.7 K (above T_N). The spectra in the temperature range 29.2–59.8 K could be fitted well in the same way as the spectrum in figure 5(a). One can observe that in the spectrum at 67.6 K (figure 6), that is close to T_N, in addition to a complex SDW Zeeman-like pattern due to Fe atoms at the 2a sites and a six-line Zeeman pattern due to Fe atoms at the 2c sites (and low-intensity Zeeman patterns due to Fe_3O_4 impurity), an asymmetric paramagnetic quadrupole

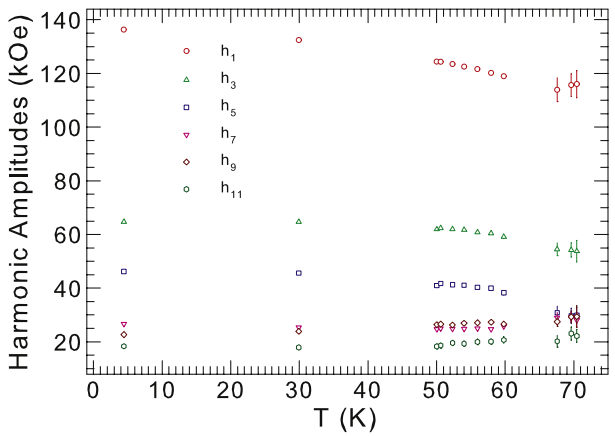

Figure 7. Temperature dependence of the harmonic amplitudes.

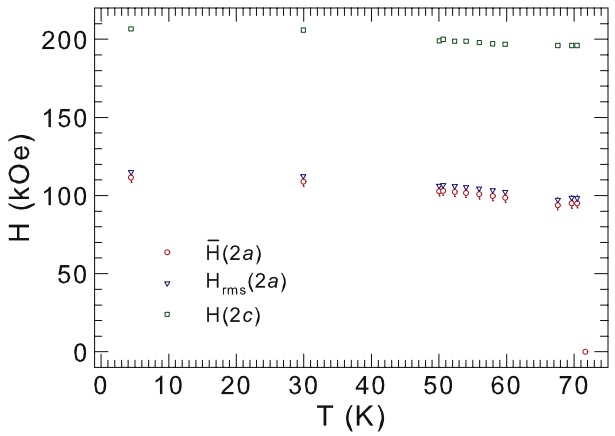

Figure 8. Temperature dependence of $\bar{H}(2a)$, $H_{\rm rms}(2a)$ and $H(2c)$.

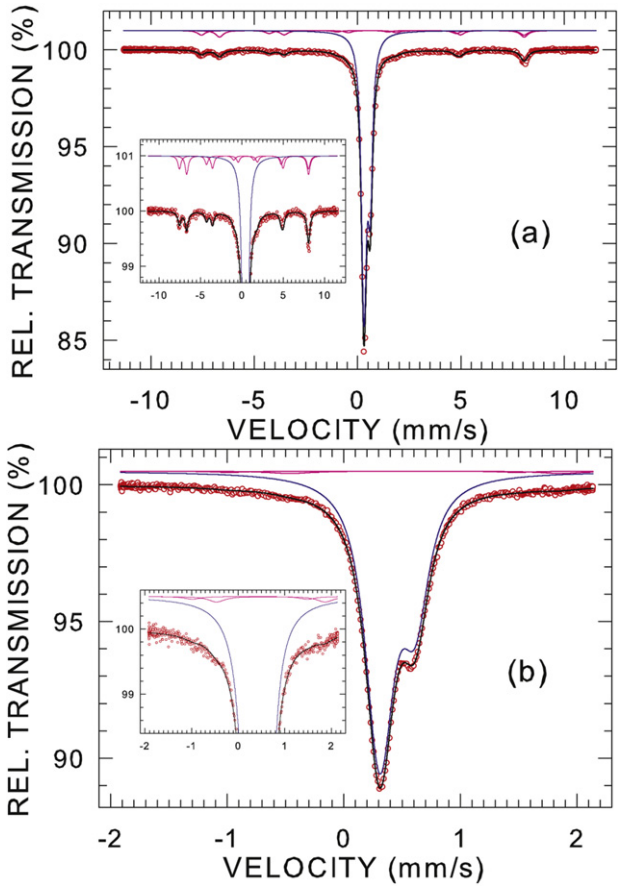

Figure 9. ^{57}Fe Mössbauer spectra of $FeSe_{0.4}Te_{0.6}$ at 297.1 K, measured in a large (a) and small (b) velocity range, fitted (black solid lines) with an asymmetric quadrupole doublet (blue solid lines) and Zeeman patterns (pink solid lines) originating from Fe_3O_4, as described in the text. The insets show the spectra with an enlarged vertical scale. The zero-velocity origin is relative to α-Fe at room temperature.

doublet (dark yellow solid line) appears, which results from the superposition of three elemental quadrupole doublets shown in figure 2(b). A quadrupole doublet component due to $FeTe_2$ impurity could not be included in the fit of the 67.6 K spectrum as it coincides with, and is completely overwhelmed by, the emerging asymmetric paramagnetic quadrupole doublet. At higher temperatures (69.6 and 70.5 K), the spectral weight of this asymmetric paramagnetic quadrupole doublet increases at the expense of the spectral weight of the Zeeman patterns originating from Fe atoms at the $2a$ and $2c$ sites, and at 71.7 K it reaches its maximum. That is, at this temperature the Zeeman patterns originating from Fe atoms at $2a$ and $2c$ sites disappear.

It can be observed from figures 5(b) and 6 that the shape of the SDW in the studied compound is almost rectangular and does not change with temperature. Good fits of the spectra in figures 5 and 6 could be achieved using $n = 6$ harmonics, and the values of the harmonic amplitudes resulting from the fits of all the spectra are shown in figure 7. The amplitude of the first harmonic h_1 is several times larger than that of the other harmonics. The amplitudes of the first three harmonics decrease slowly with increasing temperature, whereas those of the last three harmonics change very little with temperature.

The temperature dependences of the average hyperfine magnetic field (derived from the corresponding distribution $P(H)$) due to Fe atoms at the $2a$ sites $\bar{H}(2a)$, the root-mean-square hyperfine magnetic field due to Fe atoms at the $2a$ sites $H_{\rm rms}(2a)$, and the hyperfine magnetic field due to Fe atoms at the $2c$ sites $H(2c)$, are shown in figure 8. One observes a spectacularly slow decrease of these three hyperfine magnetic fields with increasing temperature, and their abrupt disappearance at ~71 K. We determine the Néel temperature to be 71.1(6) K from the observation that, at 70.5 K, $\bar{H}(2a) \neq 0$ and $H(2c) \neq 0$, but, at 71.7 K, $\bar{H}(2a) = H(2c) = 0$. Clearly, the transition at $T_{\rm N} = 71.1(6)$ K is a first-order magnetic transition.

Figure 9(a) shows the room-temperature ^{57}Fe Mössbauer spectrum of the $FeSe_{0.4}Te_{0.6}$ specimen measured over a large velocity range. Although the presence of a small amount of magnetite impurity can be detected, no contribution from the Fe_7Se_8 impurity can be seen due to its very low concentration in the studied specimen. The presence of $FeTe_2$ could not be confirmed as its quadrupole-doublet spectrum [34] overlaps with the dominant asymmetric doublet spectrum (discussed below) originating from $FeSe_{0.4}Te_{0.6}$. The room-temperature

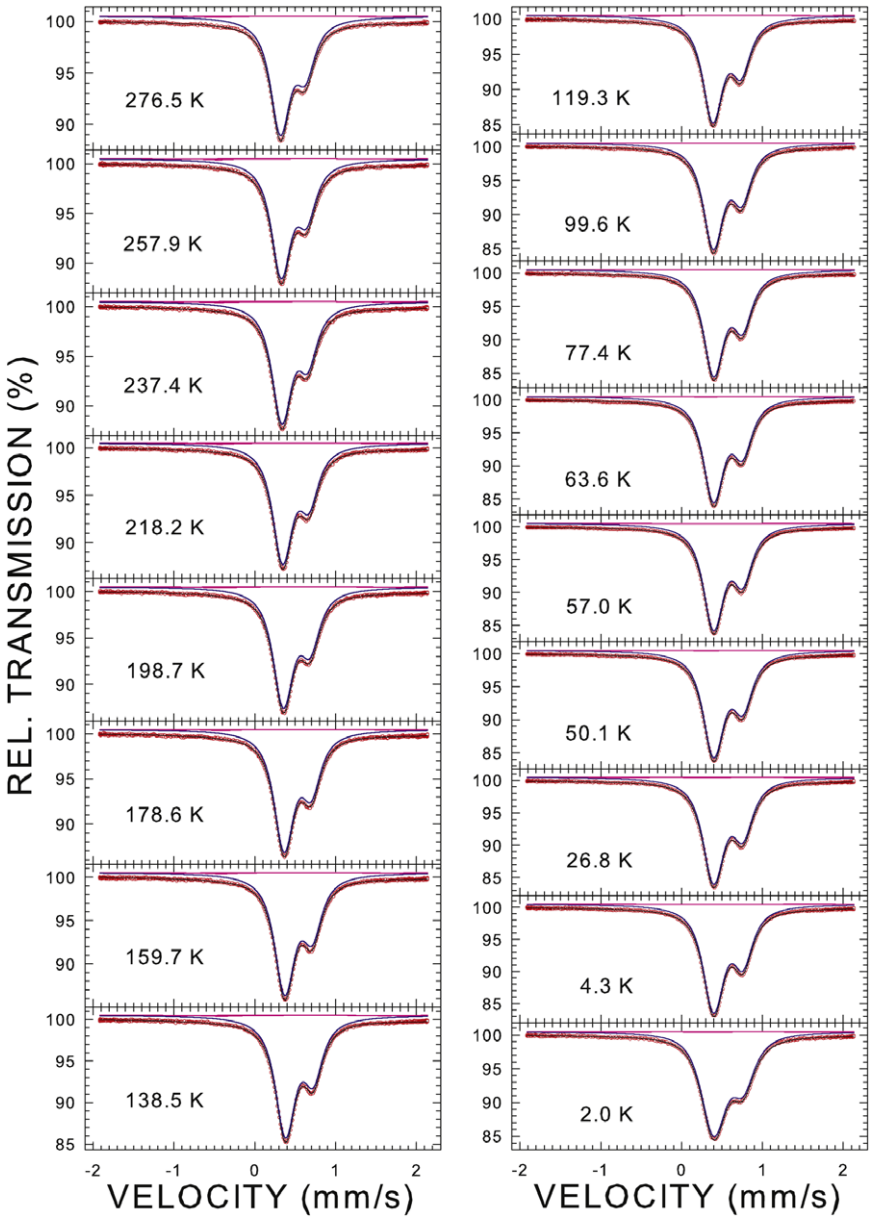

Figure 10. ^{57}Fe Mössbauer spectra of $FeSe_{0.4}Te_{0.6}$ at the indicated temperatures fitted (black solid lines) with an asymmetric quadrupole doublet (blue solid lines) and Zeeman patterns (pink solid lines) originating from Fe_3O_4, as described in the text. The zero-velocity origin is relative to α-Fe at room temperature.

^{57}Fe Mössbauer spectrum of $FeSe_{0.4}Te_{0.6}$ measured over a small velocity range (figure 9(b)) was fitted with a quadrupole doublet due to Fe atoms at 2*a* sites and a low-intensity component originating from the Fe_3O_4 impurity. The fit of this spectrum yields the quadrupole-doublet parameters that are listed in table 2.

Figure 10 shows the ^{57}Fe Mössbauer spectra of $FeSe_{0.4}Te_{0.6}$ measured at other temperatures down to 2.0 K. It is clear that no magnetic ordering occurs in the $FeSe_{0.4}Te_{0.6}$ superconductor down to 2.0 K. This confirms the earlier observations [42, 43] that replacing Te by Se in the magnetically ordered parent compound $Fe_{1+x}Te$ leads to the suppression of antiferromagnetic order and the appearance of superconductivity. These spectra were fitted (figure 10) with a quadrupole doublet originating from Fe atoms at the 2*a* sites and a very low-intensity component due to the Fe_3O_4 impurity. Figure 11(a) shows the values of Δ derived from the fits of these spectra and of the spectrum in figure 9(b). One can observe a clear increase of the magnitude of Δ with decreasing temperature. The fit of the $\Delta(T)$ data (figure 11(a)) to equation (1) gives $\Delta(0) = -0.362(1)$ mm s^{-1} and $B = 3.23(30) \times 10^{-5}$ K$^{-3/2}$.

The temperature dependence of $A(T)$, determined from the fits of the Mössbauer spectra in figures 9(b) and 10, is shown in figure 11(b). The fit of the $A(T)$ data to equation (2) yields $\Theta_D = 233(1)$ K. This value of Θ_D is larger than the values of 171 K for $FeSe_{0.4}Te_{0.6}$ [26] and 174 K for $FeSe_{0.33}Te_{0.67}$ [44] obtained from specific-heat measurements [44], but very close to the value of 230 K for

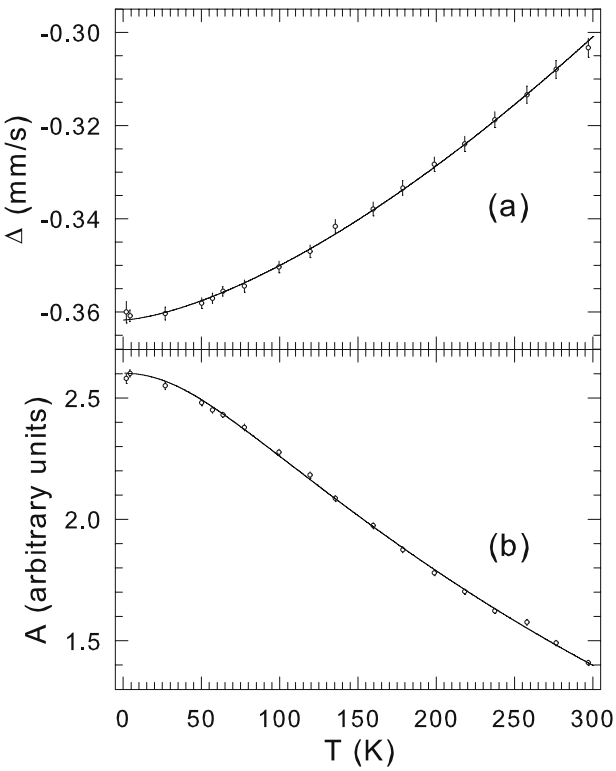

Figure 11. Temperature dependence of (a) the quadrupole splitting Δ and (b) the absorption spectral area A of $FeSe_{0.4}Te_{0.6}$. The solid lines are the fits to equation (1) in (a) and to equation (2) in (b), as explained in the text.

$FeSe_{0.42}Te_{0.58}$ that was used to calculate the experimentally observed $T_c = 14.8$ K in this superconductor [45].

4. Conclusions

We report the results of ^{57}Fe Mössbauer spectroscopy measurements in the temperature range 2–297 K of the parent compound $Fe_{1.09}Te$ and the $T_c = 14.2$ K superconductor $FeSe_{0.4}Te_{0.6}$. We find that the magnitude of the quadrupole splitting in both compounds increases with decreasing temperature according to a $T^{3/2}$ power-law relation. We demonstrate the presence of incommensurate spin-density-wave antiferromagnetism in $Fe_{1.09}Te$ and determine its Néel temperature to be 71.1(6) K. We find that the Fe magnetic moments in $Fe_{1.09}Te$ at 4.4 K at the 2*c* and 2*a* sites are, respectively, 3.20(4) and 1.78(3) μ_B, which constitutes an experimental confirmation of a theoretical prediction [11] that in the parent compound the Fe magnetic moment at the 2*c* sites should be significantly larger than that at the 2*a* sites. We confirm the absence of magnetic order in $FeSe_{0.4}Te_{0.6}$ down to 2.0 K. We find that the Debye temperatures of $Fe_{1.09}Te$ and $FeSe_{0.4}Te_{0.6}$ are 290(1) and 233(1) K, respectively.

Acknowledgments

This work was supported by the Natural Sciences and Engineering Research Council of Canada. Work at the Tohoku University was supported by a Grant-in-Aid for Scientific Research from the Japan Society for the Promotion of Science.

References

[1] Yeh K-W *et al* 2008 *Europhys. Lett.* **84** 37002
[2] Fang M H, Pham H M, Qian B, Liu T J, Vehstedt E K, Liu Y, Spinu L and Mao Z Q 2008 *Phys. Rev.* B **78** 224503
[3] Mizuguchi Y, Tomioka F, Tsuda S, Yamaguchi T and Takano Y 2009 *J. Phys. Soc. Japan* **78** 074712
[4] Mizuguchi Y, Tomioka F, Tsuda S, Yamaguchi T and Takano Y 2009 *Appl. Phys. Lett.* **94** 012503
[5] Mizuguchi Y, Deguchi K, Kawasaki Y, Ozaki T, Nagao M, Tsuda S, Yamaguchi T and Takano Y 2011 *J. Appl. Phys.* **109** 013914
[6] Grønvold F, Haraldsen H and Vihovde J 1954 *Acta Chem. Scand.* **8** 1927
[7] Chiba S 1955 *J. Phys. Soc. Japan* **10** 837
[8] Tsubokawa I and Chiba S 1959 *J. Phys. Soc. Japan* **14** 1120
[9] Westrum E F Jr, Chou C and Grønvold F 1959 *J. Chem. Phys.* **30** 761
[10] Fruchart D, Convert P, Wolfers P, Madar R, Senateur J P and Fruchart R 1975 *Mater. Res. Bull.* **10** 169
[11] Zhang L, Singh D J and Du M H 2009 *Phys. Rev.* B **79** 012506
[12] Iikubo S, Fujita M, Niitaka S and Takaji H 2009 *J. Phys. Soc. Japan* **78** 103704
[13] Bao W *et al* 2009 *Phys. Rev. Lett.* **102** 247001
[14] Li S *et al* 2009 *Phys. Rev.* B **79** 054503
[15] Martinelli A, Palenzona A, Tropeano M, Ferdeghini C, Putti M, Cimberle M R, Nguyen T D, Affronte M and Ritter C 2010 *Phys. Rev.* B **81** 094115
[16] Rodriguez E E, Stock C, Zajdel P, Krycka K L, Majkrzak C F, Zavalij P and Green M A 2011 *Phys. Rev.* B **84** 064403
[17] Zaliznyak I A, Xu Z J, Wen J S, Tranquada J M, Gu G D, Solovyov V, Glazkov V N, Zheludev A I, Garlea V O and Stone M B 2012 *Phys. Rev.* B **85** 085105
[18] Khim S, Kim J W, Choi E S, Bang Y, Nohara M, Takagi H and Kim K H 2010 *Phys. Rev.* B **81** 184511
[19] Noji T, Suzuki T, Abe H, Adachi T, Kato M and Koike Y 2010 *J. Phys. Soc. Japan* **79** 084711
[20] Aggarawal R G and Mendiratta R G 1977 *Phys. Rev.* B **16** 3908
[21] Ward J B and McCann V H 1979 *J. Phys. C: Solid State Phys.* **12** 873
[22] Gómez R W, Marquina V, Pérez-Mazariego J L, Escamilla R, Escudero R, Quintana M, Hernández-Gómez J J, Ridaura R and Marquina M L 2010 *J. Supercond. Novel Magn.* **23** 551
[23] Mizuguchi Y, Furubayashi T, Deguchi K, Tsuda S, Yamaguchi T and Takano Y 2010 *Physica* C **470** S338
Mizuguchi Y and Takano Y 2010 *J. Phys. Soc. Japan* **79** 102001
[24] Błachowski A, Ruebenbauer K, Zajdel P, Rodriguez E E and Green M A 2012 *J. Phys.: Condens. Matter* **24** 386006
[25] Taen T, Tsuchiya Y, Nakajima Y and Tamegai T 2009 *Phys. Rev.* B **80** 092502
[26] Noji T, Imaizumi M, Suzuki T, Adachi T, Kato M and Koike Y 2012 *J. Phys. Soc. Japan* **81** 054708
[27] Kawasaki Y, Deguchi K, Demura S, Watanabe T, Okazaki H, Ozaki T, Yamaguchi T, Takeya H and Takano Y 2012 *Solid State Commun.* **152** 1135
[28] Koshika Y, Usui T, Adachi S, Watanabe T, Sakano K, Simayi S and Yoshizawa M 2013 *J. Phys. Soc. Japan* **82** 023703
[29] Cali J P (ed) 1971 *Certificate of Calibration, Iron Foil Mössbauer Standard* (*Natl. Bur. Stand. (US) Circ. No. 1541*) (Washington, DC: US Government Printing Office)
[30] Greenwood N N and Gibb T C 1971 *Mössbauer Spectroscopy* (London: Chapman and Hall)

Gütlich P, Bill E and Trautwein A 2011 *Mössbauer Spectroscopy and Transition Metal Chemistry* (Berlin: Springer)

[31] Margulies S and Ehrman J R 1961 *Nucl. Instrum. Methods* **12** 131
Shenoy G K, Friedt J M, Maletta H and Ruby S L 1974 *Mössbauer Effect Methodology* vol 10, ed I J Gruverman, C W Seidel and D K Dieterly (New York: Plenum) p 277

[32] Parshall D, Chen G, Pintschovius L, Lamago D, Wolf Th, Radzihovsky L and Reznik D 2012 *Phys. Rev.* B **85** 140515(R)

[33] Häggström L, Annersten H, Ericsson T, Wäppling R, Karner W and Bjarman S 1978 *Hyperfine Interact.* **5** 201
Żukrowski J, Wiecheć A, Zach R, Tabiś W, Tarnawski Z, Król G, Kim-Ngan N-T H, Kąkol Z and Kozłowski A 2007 *J. Alloys Compounds* **442** 219
Dézsi I, Fetzer Cs, Gombkötő Á, Szűcs I, Gubicza J and Ungár T 2008 *J. Appl. Phys.* **103** 104312

[34] Ward J B, McCann V H, Quin M P L and Bates J H T 1978 *J. Phys. C: Solid State Phys.* **11** 377
Xie Y, Zhu L, Jiang X, Lu J, Zheng X, He W and Li Y 2001 *Chem. Mater.* **13** 3927

[35] Martínez-Pinedo G, Schwerdtfeger P, Caurier E, Langanke K, Nazarewich W and Söhnel T 2001 *Phys. Rev. Lett.* **87** 062701

[36] Al-Qadi K, Wang P, Stadnik Z M and Przewoźnik J 2009 *Phys. Rev.* B **79** 224202 and references therein

[37] Chen G F, Chen Z G, Dong J, Hu W Z, Li G, Zhang X D, Luo J L and Wang N L 2009 *Phys. Rev.* B **79** 140509(R)

[38] Street R, Munday B C, Window B and Williams I R 1968 *J. Appl. Phys.* **39** 1050

[39] Cieślak J and Dubiel S M 1995 *Nucl. Instrum. Methods Phys. Res.* B **95** 131 and references therein

[40] Bonville P, Rullier-Albenque F, Colson D and Forget A 2010 *Europhys. Lett.* **89** 67008

[41] Panissod P, Durand J and Budnik J I 1982 *Nucl. Instrum. Methods* **199** 99
Panissod P 1985 *Hyperfine Interact.* **24–26** 607
Eriksson O and Svane A 1989 *J. Phys.: Condens. Matter* **1** 1589
Dubiel S M 2009 *J. Alloys Compounds* **488** 18

[42] Wen J, Xu G, Gu G, Tranquada J M and Birgenau R J 2011 *Rep. Prog. Phys.* **74** 124503 and references therein

[43] Malavasi L and Margadonna S 2012 *Chem. Soc. Rev.* **41** 3897 and references therein

[44] Sales B C, Sefat A S, McGuire M A, Jin R Y, Mandrus D and Mozharivskyj Y 2009 *Phys. Rev.* B **79** 094521

[45] Cho K, Kim H, Tanatar M A, Hu J, Qian B, Mao Z Q and Prozorov R 2011 *Phys. Rev.* B **84** 174502